Author Manuscript

Author Manuscript

Author Manuscript

Author Manuscript

HHS Public Access

Author manuscript

J Bone Miner Res. Author manuscript; available in PMC 2016 July 27.

Published in final edited form as:

J Bone Miner Res. 2014 December ; 29(12): 2643–2652. doi:10.1002/jbmr.2284.

FTIR-I Compositional Mapping of the Cartilage-to-Bone Interface as a Function of Tissue Region and Age

Nora T Khanarian[1], **Margaret K Boushell**[1], **Jeffrey P Spalazzi**[1], **Nancy Pleshko**[2,a], **Adele L Boskey**[2], and **Helen H Lu**[1]

[1]Biomaterials and Interface Tissue Engineering Laboratory, Department of Biomedical Engineering, Columbia University, New York, NY, USA

[2]Musculoskeletal Integrity Program, Hospital for Special Surgery, New York, NY, USA

Abstract

Soft tissue-to-bone transitions, such as the osteochondral interface, are complex junctions that connect multiple tissue types and are critical for musculoskeletal function. The osteochondral interface enables pressurization of articular cartilage, facilitates load transfer between cartilage and bone, and serves as a barrier between these two distinct tissues. Presently, there is a lack of quantitative understanding of the matrix and mineral distribution across this multitissue transition. Moreover, age-related changes at the interface with the onset of skeletal maturity are also not well understood. Therefore, the objective of this study is to characterize the cartilage-to-bone transition as a function of age, using Fourier transform infrared spectroscopic imaging (FTIR-I) analysis to map region-dependent changes in collagen, proteoglycan, and mineral distribution, as well as collagen organization. Both tissue-dependent and age-related changes were observed, underscoring the role of postnatal physiological loading in matrix remodeling. It was observed that the relative collagen content increased continuously from cartilage to bone, whereas proteoglycan peaked within the deep zone of cartilage. With age, collagen content across the interface increased, accompanied by a higher degree of collagen alignment in both the surface and deep zone cartilage. Interestingly, regardless of age, mineral content increased exponentially across the calcified cartilage interface. These observations reveal new insights into both region- and age-dependent changes across the cartilage-to-bone junction and will serve as critical benchmark parameters for current efforts in integrative cartilage repair.

Keywords

COLLAGEN; MATRIX MINERALIZATION; OSTEOARTHRITIS; BIOENGINEERING; AGING

Address correspondence to: Helen H Lu, PhD, Department of Biomedical Engineering, Columbia University, 351 Engineering Terrace Building, MC 8904, 1210 Amsterdam Avenue, New York, NY 10027, USA. hhlu@columbia.edu.

[a]Present address: Department of Bioengineering, Temple University, Philadelphia, PA, USA

Disclosures

All authors state that they have no conflicts of interest.

Authors' roles: Study design: NK, AB, and HL. Study conduct: NK and JS. Data collection: NK. Data analysis: NK, JS, and MB. Data interpretation: NK, JS, AB, and HL. Drafting manuscript: NK. Revising manuscript content: NK, MB, NP, AB, and HL. Approving final version of manuscript: NK, MB, JS, NP, AB, and HL. NK takes responsibility for the integrity of the data analysis.

Author Manuscript Author Manuscript Author Manuscript Author Manuscript

Introduction

Complex biological interfaces enable integration of soft and hard tissues and are essential for musculoskeletal function. One of these critical interfaces is located at the osteochondral junction, where articular cartilage transitions into subchondral bone through a calcified cartilage layer. This calcified cartilage transition is approximately 50 to 250μm in humans,[1,2] varying with age and relative in depth to overall cartilage thickness. The interface is composed of hypertrophic chondrocytes embedded in a calcified, proteoglycan-containing matrix,[3] which is also rich in collagen II.[4–6] The mineral phase of calcified cartilage is a carbonate-substituted form of hydroxyapatite, with similar chemistry and crystal size to the mineral in bone.[7] Collagen type X,[6,8] which regulates cell-mediated mineral deposition by hypertrophic chondrocytes, is also present in the calcified cartilage matrix.

The osteochondral interface allows for structural continuity between cartilage and bone, while maintaining the integrity of each tissue region.[9] Additionally, it serves as a physical barrier that restricts transport,[10,11] representing at least a fivefold decrease in permeability compared with articular cartilage.[12] It also prevents vascular invasion from subchondral bone into the cartilage compartment[13] and allows for pressurization during loading.[14] Moreover, the modulus of human calcified cartilage layer is intermediate in magnitude between articular cartilage and bone.[15] This gradation of tissue mechanical properties enables force transmission across the joint and reduces stress concentrations at the osteochondral interface.[16,17]

Although the osteochondral junction has been extensively described using histological and microscopy methods,[1–3,17–27] quantitative characterization via conventional techniques has been challenging because of the structural complexity and relatively small scale of the interface. The novel method of infrared spectroscopic imaging uses the vibrational modes of specific molecular components to generate high-resolution maps of the composition, distribution, and organization of matrix components. To date, both Fourier transform infrared spectroscopic imaging (FTIR-I) and Raman spectroscopy have been used to analyze a variety of connective tissues, including bone,[28–31] articular cartilage,[32–38] and healing cartilage,[39] and has also been useful for studying complex tissue transitions such as the ligament-to-bone[40] and tendon-to-bone[41,42] interfaces. Specifically, IR imaging is a high-resolution and high-throughput technique that is especially advantageous for characterizing inhomogeneities or spatial changes across multiple tissue types. This technique has been shown to correlate directly with histological and quantitative analyses of the cartilage matrix[43,44] and is not limited by the inherent shortcomings of histology, such as batch-to-batch variations in staining solutions and qualitative interpretation of stains. Strong correlation has also been reported between FTIR-I measurements and biochemical quantification of collagen and proteoglycan content.[43] Furthermore, the ratio of amide I to amide II band areas can be used to determine collagen fiber orientation.[45] In short, FTIR-I is a powerful technique for concurrent analysis of multiple extracellular matrix components within the same sample, making it the optimal method for mapping multitissue transitions such as the cartilage-to-bone junction.

Author Manuscript Author Manuscript Author Manuscript Author Manuscript

In this study, the first objective is to use FTIR-I to investigate region-dependent changes in collagen, proteoglycan, and mineral distribution from articular cartilage to calcified cartilage and to bone. Because the calcified cartilage interface resides between the soft and hard tissues, it is anticipated that its extracellular matrix composition will be intermediate between those of articular cartilage and bone. The second objective of this study is to determine age-dependent differences in matrix and mineral distribution across the osteochondral interface, focusing on changes that occur during postnatal development with the onset of skeletal maturity. Although age-related comparisons have been reported for articular cartilage,[46] no systematic analysis of the osteochondral interface pre- and post-skeletal maturity has been reported. Given the functional differences between immature and mature cartilage, structural changes in terms of individual matrix components at the interface are expected. In addition to providing new insights into the maturation of the osteochondral interface, the results of this study will yield benchmark parameters for evaluating the success of tissue-engineered cartilage or osteochondral grafts.

Materials and Methods

Sample isolation and preparation

Osteochondral samples were isolated from bovine tibiofemoral joints ($n = 3$, Green Village Packing Company, Green Village, NJ, USA), which represent a well-characterized large animal model.[32,47–51] Healthy bovine specimens can be readily obtained and, unlike the rodent model, reflect skeletal maturity and closure of the growth plate similar to what is observed in humans. Furthermore, the majority of FTIR-I studies have been conducted using the bovine model, enabling us to validate our approach and compare current findings with published studies.[32,36] Briefly, a sterile biopsy punch was used to extract osteochondral plugs (6 × 4 mm, $n = 3$/group) from the tibial plateaus of immature joints, whereas a bandsaw was used to isolate mature plugs (10 × 10 mm, $n = 3$/group). Each sample was halved for corresponding decalcified and nondecalcified analyses. For decalcification, osteochondral plugs were immediately fixed for 24 hours with 80% ethanol, supplemented with 1% cetylpyridinium chloride (CPC, Sigma, St. Louis, MO, USA) to preserve proteoglycans.[52] After fixation, samples were rinsed in distilled water before demineralization in tris-hydroxymethylaminomethane buffer (Tris, Sigma) containing 10% ethylenediaminetetraacetic acid (EDTA, Sigma). Samples were then dehydrated using an ethanol series, cleared with xylene, and embedded in paraffin (Fisher Scientific, Pittsburgh, PA, USA). The samples were sectioned (Reichert-Jung RM 2030 Microtome, Leica, Bannockburn, IL, USA; 7 μm) and placed immediately between barium fluoride optical windows (Spectral Systems, Hopewell Junction, NY, USA). The sections were deparaffinized in xylene, dehydrated with an ethanol series, and then dried overnight under vacuum. A second barium fluoride window was placed over the sample before infrared analysis. Corresponding sections were stained with alcian blue and picrosirius red to visualize glycosaminoglycans and collagen distribution, respectively. Collagen orientation was imaged with light microscopy using a polarized light filter (Olympus BX60, Olympus, Center Valley, PA, USA).

Author Manuscript Author Manuscript Author Manuscript Author Manuscript

The nondecalcified samples were fixed after isolation with 90% ethanol for 24 hours, followed by embedding in polymethylmethacrylate (PMMA, Sigma).[53] Combining ethanol fixation with PMMA embedding has been shown to minimize interference owing to fixation and embedding.[54] The samples were sectioned (2 μm) with a Leica sliding microtome (SM2500S, Leica Microsystems Inc.) using a tungsten carbide blade (Delaware Diamond Knives Inc., Wilmington, DE, USA). Individual sections were dried and placed between barium fluoride windows for FTIR-I analysis. Corresponding sections were stained via von Kossa[51] to visualize mineral distribution and compare with FTIR-I analysis.

Fourier transform infrared imaging

FTIR-I analysis was performed using an FTIR spectrometer (Spectrum 100, Perkin Elmer, Waltham, MA, USA) coupled to a microscope imaging system (Spotlight 300, Perkin Elmer). The spectra were acquired with a spectral resolution of 8 cm^{-1} and a spatial resolution of 6.25 μm. The distribution of collagen and proteoglycan were mapped using the amide I (1720 to 1590 cm^{-1}) and carbohydrate (1140 to 985 cm^{-1}) peaks, respectively, whereas mineral distribution was characterized using the phosphate band (1200 to 900 cm^{-1}). Although more recent studies have shown some improvement in specificity of proteoglycan assessment using multivariate methodology,[55] the proteoglycan parameters used in the current study have been validated by correlation to both biochemical and histology data.[43,56] Because the carbohydrate and phosphate peaks overlap in the IR spectra, decalcified samples were used for matrix analysis, whereas the corresponding calcified samples were used for mineral analysis. Note that the contribution of the carbohydrate peak in the calcified sections was negligible compared with the phosphate peak. For each sample, regions of interest (~750 × 1750μm/region) containing cartilage, calcified cartilage, and bone were scanned, and ~8000 points of spectral data were acquired per region, constituting a total of ~24,000 spectra collected per sample.

Spectra analyses

The IR spectra were analyzed and spectroscopic maps were generated using ISYS 3.1.1 chemical imaging software (Spectral Dimensions Inc., Olney, MD, USA) and MATLAB 7.0 R14 (The MathWorks Inc., Natick, MA, USA). Before analysis, spectra were background corrected by baseline subtraction. Signature peaks within the collagen and proteoglycan spectra have been shown to be linearly proportional to collagen and proteoglycan content.[32] Therefore, relative collagen distribution ($n = 3$) was determined by integrating the peak area under the amide I band (1720 to 1590 cm^{-1}), and proteoglycan distribution ($n = 3$) was estimated by integrating the peak area under a carbohydrate band associated with C-O-C and C-OH vibrations (1140 to 985 cm^{-1}).[32]

Additionally, collagen alignment ($n = 3$) was determined by scanning the demineralized samples with a gold-wire polarizer grid (Perkin Elmer, Shelton, CT, USA) inserted in the path of the IR light, with the polarizer aligned at 0° with respect to the interface between cartilage and bone. Because amide I and amide II bond vibrations are orthogonal, the ratio of their band areas is an indicator of collagen fibril orientation when spectra are collected with polarized light.[45] Therefore, in this study, spectra obtained with the polarizer were integrated under the amide I (1720 to 1590 cm^{-1}) and amide II bands (1590 to 1492 cm^{-1}),

Author Manuscript Author Manuscript Author Manuscript Author Manuscript

and numerical indices for collagen orientation were obtained by calculating the ratio between their bands. A band ratio ≥2.7 is indicative of fibril orientation parallel to the interface, and when the ratio is ≤1.7, the fibers are perpendicular to the interface. A ratio ranging from 1.7 to 2.7 reflects mixed fibril orientation.

The relative mineral-to-matrix ratio ($n = 3$) in each tissue region was calculated by integrating under the *v1*, *v3* phosphate band contour (1200 to 900 cm^{-1}) and dividing by the amide I band area.[54] Before analysis of mineral distribution, the collected spectra were corrected for contributions from PMMA embedding. To this end, spectra of pure PMMA were acquired, baseline corrected, and normalized by the highest peak in the PMMA spectrum (1728 cm^{-1}). Sample spectra were likewise baseline corrected and normalized. The PMMA spectrum was then subtracted from the sample spectra to eliminate the background from embedding. This method of normalization and subtraction was implemented to compensate for different degrees of PMMA penetration into the multiple tissue types evaluated across the interface. Additionally, the normalized carbonate content ($n = 3$) in the apatite structure was estimated from the carbonate-to-matrix ratio, determined by integrating under the carbonate *v2* band (890 to 850 cm^{-1}) and dividing by the area of the amide I band, which accounts for any potential variations in sample thickness.

Line profiles of collagen, proteoglycan, and mineral distribution from the articular surface to bone were generated based on spectra data, and corresponding histology staining was used to demarcate articular cartilage, calcified cartilage, and bone regions. Line profiles were performed repeatedly across the interface spectroscopic maps on a pixel-by-pixel basis and then averaged, resulting in a single average line profile representing all the data collected for the osteochondral region. Regions exhibiting anomalies such as holes or folds in the sections were excluded. Normalized distance, calculated as distance divided by total sample distance, was used to account for differences in thickness between osteochondral specimens. The relative values for matrix and mineral were also calculated for each tissue region examined, namely articular cartilage (AC), calcified cartilage (CC), and bone.

Statistical analyses

Results are presented in the form of mean ± standard deviation, with *n* equal to the number of animals analyzed per group. Two-way analysis of variance (ANOVA), followed by a Tukey-HSD post hoc test was performed to determine region- and age-dependent differences in relative matrix and mineral content ($p < 0.05$). Statistical analysis was performed using the JMP statistical software package (version 4.0, SAS Institute, Cary, NC, USA). In addition, within the calcified cartilage region, relative mineral content was plotted against normalized distance across the interface, and the raw data was fit to both linear ($y = Ax + B$) and exponential ($y = Ce^{D} + E$) curves.

Results

Sample size and spectra analyses

Regardless of age, articular cartilage spanned approximately 60% of the total tissue height, or 991 ± 51μm and 1044 ± 275μm for immature and mature specimens, respectively. For

Author Manuscript Author Manuscript Author Manuscript Author Manuscript

each age group, cartilage was also subdivided into the surface (10%), middle (25%), and deep zones (25%), based on established characterization studies of articular cartilage.[21] On average, the calcified cartilage region spanned approximately 10% of the total sample height, or 165 ± 8μm for immature samples and 174 ± 46μm for mature samples. Each sample tested contained approximately 30% bone by height, which translated into 496 ± 25μm for immature samples and 522 ± 138μm for mature specimens. No statistical differences in total or region-specific dimensions were found between immature and mature samples. Representative spectra from articular cartilage (AC), calcified cartilage (CC), and subchondral bone are shown in Fig. 1*B*. Whereas the amide I, amide II, and carbohydrate peaks were present in all tissue regions, the phosphate band was observed only at the calcified cartilage and bone regions.

Collagen distribution and orientation

As shown in Fig. 2, quantitative mapping of the immature samples revealed continuous tissue regions, with an increase in collagen content across the interface. The lowest amount of collagen was found at the region closest to the articular surface ($p < 0.05$), although no difference in collagen content was found between middle and deep zone cartilage, calcified cartilage, or bone regions. Interestingly, collagen fibrils in the middle zone of immature articular cartilage were organized parallel (0°) to the calcified cartilage region (Fig. 2), with no apparent deep zone orientation. Similarly, no apparent alignment was detected within the calcified cartilage region in the immature samples.

For the mature samples, the line scans also reveal increasing collagen content progressing from the articular surface to bone (Fig. 2), with significantly higher collagen detected in the deep zone, calcified cartilage, and bone compared with the surface zone cartilage. Both the calcified cartilage and bone contained significantly more collagen compared with the middle zone of cartilage. In contrast, no significant difference in relative collagen content was found among deep zone cartilage, calcified cartilage, and bone. The collagen fibrils of mature samples were highly oriented parallel to the articular surface in the surface zone and perpendicular to the calcified cartilage region in the deep zone, typical of articular cartilage structure (Fig. 2). In the calcified cartilage region, a relatively random collagen orientation was detected compared with the deep zone. With age, collagen orientation increased in the surface and deep zone regions of cartilage, and the mature samples also contained significantly more collagen compared with immature samples in both the surface and deep zones (Fig. 2). Similarly, a higher collagen content was also measured in the calcified cartilage and bone regions of mature samples compared with immature samples ($p < 0.05$). Finally, both immature and mature samples exhibited little change in collagen content within the calcified cartilage region (Fig. 5).

Proteoglycan distribution

For the immature samples, the relative amount of proteoglycan remained constant across the cartilage-to-bone junction (Fig. 3). The surface zone measured a lower proteoglycan content than the middle or deep zone of articular cartilage, as well as the calcified cartilage region ($p < 0.05$). No significant difference was found between the middle zone, deep zone, and calcified cartilage regions. As expected, there was significantly less proteoglycan in

Author Manuscript Author Manuscript Author Manuscript Author Manuscript

subchondral bone compared with the deep zone and calcified cartilage. When the carbohydrate peak (1140 to 985 cm^{-1}) was normalized by the amide I peak (1720 to 1590 cm^{-1}) to determine the relative proteoglycan distribution with respect to collagen, the average proteoglycan content was found to be the highest in the surface and deep zones ($p < 0.05$, Fig. 3).

For the mature samples, the line scan shows peak proteoglycan content at the articular cartilage-to-calcified cartilage interface. A lower proteoglycan content was measured in the surface zone compared with the deep zone ($p < 0.05$), whereas no difference in proteoglycan content was found between the middle zone, deep zone, calcified cartilage, and bone regions. Furthermore, there was no significant difference in normalized proteoglycan content between any of the regions (Fig. 3). When comparing the immature and mature groups, significantly higher proteoglycan content was present in the deep zone of mature samples (Fig. 3). No other age-dependent differences were evident between tissue zones. Finally, in terms of proteoglycan content within the calcified cartilage region itself (Fig. 5), proteoglycan content decreased linearly in mature samples ($R^2 = 0.93 \pm 0.05$), whereas no such trend was evident for immature samples.

Mineral distribution

For the immature samples, all three zones of articular cartilage were essentially mineral-free (Fig. 4), whereas in the calcified tissue regions, the mineral content of the calcified cartilage region was significantly lower than that of bone with more mineral detected in calcified cartilage and bone regions for all samples evaluated ($p < 0.05$, Fig. 5). The line scans of normalized mineral distribution demonstrate both linear ($R^2 = 0.89 \pm 0.06$) and exponential ($R^2 = 0.98 \pm 0.01$) fits of the transition within the calcified cartilage region. However, the R^2 value of the exponential fit was significantly higher than the R^2 value of the linear fit. The carbonate peak (890 to 850 cm^{-1}) was only detected in the calcified cartilage region.

For the mature samples, the articular cartilage region was similarly mineral-free (Fig. 4), whereas the calcified cartilage region again measured a significantly lower normalized mineral content than bone (Fig. 5). The line scans of normalized mineral distribution follow both linear ($R^2 = 0.93 \pm 0.03$) and exponential ($R^2 = 0.97 \pm 0.01$) fits of the transition region from uncalcified cartilage to bone, although the R^2 values were not significantly different between fits. When comparing the immature and mature groups, although no significant difference in normalized mineral content was detected in the calcified cartilage region (Fig. 4), a significantly lower relative mineral content was found in the bone region of the mature samples ($p < 0.05$).

Discussion

The critical junction between cartilage and bone consists of a region of calcified cartilage tissue that facilitates soft-to-hard tissue integration, allows for pressurization during loading, serves as a barrier to vascular invasion, and enables cartilage loading. Using FTIR-I, this study represents the first comprehensive analysis of all tissue regions progressing from cartilage to bone and as a function of age, focusing on postnatal characterization of the relative content, distribution, and organization of key matrix components across the soft and

Author Manuscript Author Manuscript Author Manuscript Author Manuscript

hard tissue regions. Both region- and age-dependent changes in collagen, proteoglycan, and mineral content and distribution, as well as collagen orientation, were observed across the cartilage-to-bone junction.

In terms of matrix distribution, the results of this study reveal that the spatial content of collagen and proteoglycan differ across the cartilage zones, as well as the calcified cartilage and bone regions. It was observed that before skeletal maturity, articular cartilage consists of a clearly delineated surface region with the lowest matrix content, followed by the middle and deep zones with relatively higher proteoglycan and collagen content. A similar trend progressing from the articular surface to the deep zone was seen in the mature group. Overall, these results are in agreement with published biochemical analyses,[46] which reported a depth-dependent increase in proteoglycan and collagen content for both immature and mature bovine cartilage. Similarly for subchondral bone and in agreement with previous studies,[57,58] a mineral- and collagen-rich matrix with a relatively low proteoglycan content was found. In this study, mature samples measure more collagen in the surface and deep zone, as well as a greater amount of proteoglycan in the deep zone. Similar increases in matrix content with age have also been reported when comparing fetal and newborn bovine articular cartilage.[46] In addition, distinct changes in collagen fiber organization are observed with age. Although only collagen fibers in the middle zone of the immature group are oriented parallel to the interface, there is an increase in collagen orientation for the mature group; fibrils are parallel to the articular surface in the surface zone and perpendicular to bone in the deep zone. The gradual assembly of the collagen network and parallel biochemical changes in postnatal tissue marks the transition from a relatively homogenous tissue toward an organized mature interface. It has been reported that although collagen is randomly oriented in fetal articular cartilage tissue, its organization increases with age,[59,60] likely related to the onset of physiological loading.[51,61] Additionally, collagen maturity is another important characteristic of the matrix and will be examined in future studies.

For the calcified cartilage region, it was observed that regardless of age and with the exception of mineral content, its collagen and proteoglycan content are comparable to those of deep zone cartilage. Interestingly, collagen lacks organization in the calcified cartilage layer, which is in agreement with electron microscopy results that documented a transition from highly oriented collagen fibers in cartilage to randomly oriented fibers at the osteochondral interface in human samples.[19] Across the calcified cartilage region, mineral content increases exponentially for both the immature and mature groups. Interestingly, this is reminiscent of other soft tissue-to-bone interfaces such as the immature anterior cruciate ligament insertion site, which also exhibits an exponential gradient in mineral content from mineralized fibrocartilage to bone.[40] It is emphasized that the observed gradient in mineral content is intrinsic to this interface because both unnormalized and normalized mineral distributions were examined and yielded similar results. In addition, these findings are in agreement with the results of Gupta and colleagues, where quantitative back-scattered electron imaging of adult human osteochondral samples revealed a sharp increase in mineral content over a span of 30-μmregion within the uncalcified-to-calcified cartilage transition;[62] the average calcium content of human calcified cartilage varied significantly

Author Manuscript Author Manuscript Author Manuscript Author Manuscript

(1% to 28% dry weight), whereas that of subchondral bone was more consistent (16% to 26%).

The depth-dependent changes in matrix and mineral content across the osteochondral interface are also mirrored by changes in mechanical properties,[46,48,50] and these structure-function relationships are critical to understanding both normal and diseased joint conditions. Correlations between matrix content (proteoglycan and collagen) and cartilage mechanical properties (compressive and shear strength, respectively) have been established, indicating that the depth-dependent mechanical profile through the surface, middle, and deep zones can be attributed to the depth-dependent changes in the cartilage matrix content and organization.[46,63,64] Interestingly, the findings of this study suggest that the region-dependent changes in proteoglycan and collagen content do not fully explain the order of magnitude differences found in compressive moduli across the osteochondral interface. Given that a positive correlation also exists between mineralization and indentation modulus in mature human calcified cartilage and subchondral bone samples,[65] it is more likely that the exponential increase in mineral content significantly enhances calcified cartilage mechanical properties. Moreover, the role of GAG- and collagen-mineral interactions may also be important for engineering the mechanics of calcified cartilage and will be investigated in future studies.

In addition to identifying region- and age-related changes at the cartilage-to-bone junction, findings from this study also yield benchmark criteria for cartilage and osteochondral tissue engineering,[66,67] as well as revealing new insights into the postnatal maturation process that is critical for the long-term success of tissue-engineering strategies. The exponential increase from basal to high mineral content, as opposed to a linear gradient, suggests that this transition can be recapitulated in a biomimetic design as structurally continuous scaffold phases with a stepwise increase in mineral content, ie, mineral-free contiguous with mineral-containing regions. Furthermore, the calcified cartilage matrix is collagen- and proteoglycan-rich, with matrix content and distribution resembling that of the non-mineralized deep zone cartilage. Therefore, tissue-engineering strategies aimed at regeneration of the osteochondral interface would focus on the formation of deep zone cartilage-like tissue within a mineral-containing matrix, and achieving desired matrix organization by postnatal physiological loading either inherent in vivo or introduced ex vivo via bioreactor culture. Future studies will build on these results to elucidate disease-related changes in matrix distribution and organization across the soft-to-hard tissue transition, as well as extend these quantitative analyses to human samples.

Characterization of matrix and mineral distribution across the osteochondral interface, spanning articular cartilage, calcified cartilage, and bone tissue, is critical for elucidating structure-function relationships and devising biomimetic strategies for complex tissue regeneration. Quantitative mapping has revealed both region- and age-dependent changes within the tissue transition from cartilage to bone. Moreover, mineral is localized to calcified cartilage and bone, and its distribution is characterized by an exponential increase in mineral content from calcified cartilage to bone. These trends in mineral distribution are maintained with age, accompanied by a higher overall collagen content and increased fiber organization at the mature cartilage-to-bone junction.

Author Manuscript Author Manuscript Author Manuscript Author Manuscript

Acknowledgments

The authors thank Ms Lyudmila Spevak at the Hospital for Special Surgery for assistance with data acquisition and analysis. This study was supported by the Presidential Early Career Award for Scientists and Engineers (HHL), NIH-NIAMS (AR052402, HHL), HSS Core Center Grant (AR046121, ALB), the National Science Foundation Graduate Research Fellowship (NTK), the Columbia Technology Innovation and Community Engagement Fellowship (MKB), and the NIH Ruth L. Kirschstein National Research Service Award T32 (AR059038, NTK, MKB).

References

1. Lane LB, Bullough PG. Age-related changes in the thickness of the calcified zone and the number of tidemarks in adult human articular cartilage. J Bone Joint Surg Br. 1980; 62:372–5. [PubMed: 7410471]
2. Muller-Gerbl M, Schulte E, Putz R. The thickness of the calcified layer of articular cartilage: a function of the load supported? J Anat. 1987; 154:103–11. [PubMed: 3446655]
3. Bullough PG, Jagannath A. The morphology of the calcification front in articular cartilage. Its significance in joint function. J Bone Joint Surg Br. 1983; 65:72–8. [PubMed: 6337169]
4. Roberts S. Collagen of the calcified layer of human articular cartilage. Experientia. 1985; 41:1138–9. [PubMed: 3899713]
5. Buckwalter JA, Rosenberg LC, Ungar R. Changes in proteoglycan aggregates during cartilage mineralization. Calcif Tissue Int. 1987; 41:228–36. [PubMed: 3119178]
6. Boskey AL. Mineral-matrix interactions in bone and cartilage. Clin Orthop Relat Res. 1992; 281:244–74. [PubMed: 1323440]
7. Duer MJ, Friscic T, Murray RC, Reid DG, Wise ER. The mineral phase of calcified cartilage: its molecular structure and interface with the organic matrix. Biophys J. 2009; 96:3372–8. [PubMed: 19383480]
8. Eyre D. Collagen of articular cartilage. Arthritis Res. 2002; 4:30–5. [PubMed: 11879535]
9. Hunziker EB, Driesang IM, Saager C. Structural barrier principle for growth factor-based articular cartilage repair. Clin Orthop Relat Res. 2001; 391(Suppl):S182–9. [PubMed: 11603703]
10. Arkill KP, Winlove CP. Solute transport in the deep and calcified zones of articular cartilage. Osteoarthritis Cartilage. 2008; 16:708–14. [PubMed: 18023368]
11. Pan J, Zhou X, Li W, Novotny JE, Doty SB, Wang L. In situ measurement of transport between subchondral bone and articular cartilage. J Orthop Res. 2009; 27:1347–52. [PubMed: 19360842]
12. Mauck RL, Hung CT, Ateshian GA. Modeling of neutral solute transport in a dynamically loaded porous permeable gel: implications for articular cartilage biosynthesis and tissue engineering. J Biomech Eng. 2003; 125:602–14. [PubMed: 14618919]
13. Walsh DA, Bonnet CS, Turner EL, Wilson D, Situ M, McWilliams DF. Angiogenesis in the synovium and at the osteochondral junction in osteoarthritis. Osteoarthritis Cartilage. 2007; 15:743–51. [PubMed: 17376709]
14. Soltz MA, Ateshian GA. Experimental verification and theoretical prediction of cartilage interstitial fluid pressurization at an impermeable contact interface in confined compression. J Biomech. 1998; 31:927–34. [PubMed: 9840758]
15. Mente PL, Lewis JL. Elastic modulus of calcified cartilage is an order of magnitude less than that of subchondral bone. J Orthop Res. 1994; 12:637–47. [PubMed: 7931780]
16. Oegema, TR., Jr; Thompson, RC, Jr. Cartilage-bone interface (tidemark). In: Brandt, KD., editor. Cartilage changes in osteoarthritis. Indianapolis: Indiana School of Medicine Publ; 1990. p. 43-52.
17. Oegema TR Jr, Carpenter RJ, Hofmeister F, Thompson RC Jr. The interaction of the zone of calcified cartilage and subchondral bone in osteoarthritis. Microsc Res Tech. 1997; 37:324–32. [PubMed: 9185154]
18. Broom ND, Poole CA. A functional-morphological study of the tidemark region of articular cartilage maintained in a non-viable physiological condition. J Anat. 1982; 135:65–82. [PubMed: 7130057]

Author Manuscript Author Manuscript Author Manuscript Author Manuscript

19. Hough AJ, Banfield WG, Mottram FC, Sokoloff L. The osteochondral junction of mammalian joints. An ultrastructural and microanalytic study. Lab Invest. 1974; 31:685–95. [PubMed: 4215924]
20. Oettmeier R, Abendroth K, Oettmeier S. Analyses of the tidemark on human femoral heads. II. Tidemark changes in osteoarthrosis—a histological and histomorphometric study in non-decalcified preparations. Acta Morphol Hung. 1989; 37:169–80. [PubMed: 2486460]
21. Hunziker EB, Quinn TM, Hauselmann HJ. Quantitative structural organization of normal adult human articular cartilage. Osteoarthritis Cartilage. 2002; 10:564–72. [PubMed: 12127837]
22. Green WT Jr, Martin GN, Eanes ED, Sokoloff L. Microradiographic study of the calcified layer of articular cartilage. Arch Pathol. 1970; 90:151–8. [PubMed: 5433599]
23. Lane LB, Villacin A, Bullough PG. The vascularity and remodelling of subchondrial bone and calcified cartilage in adult human femoral and humeral heads. An age- and stress-related phenomenon. J Bone Joint Surg Br. 1977; 59:272–8. [PubMed: 893504]
24. Havelka S, Horn V, Spohrova D, Valouch P. The calcified-noncalcified cartilage interface: the tidemark. Acta Biol Hung. 1984; 35:271–9. [PubMed: 6242456]
25. Norrdin RW, Kawcak CE, Capwell BA, McIlwraith CW. Calcified cartilage morphometry and its relation to subchondral bone remodeling in equine arthrosis. Bone. 1999; 24:109–14. [PubMed: 9951778]
26. Lyons TJ, McClure SF, Stoddart RW, McClure J. The normal human chondro-osseous junctional region: evidence for contact of uncalcified cartilage with subchondral bone and marrow spaces. BMC Musculoskelet Disord. 2006; 7:52. [PubMed: 16787529]
27. Clark JM, Huber JD. The structure of the human subchondral plate. J Bone Joint Surg Br. 1990; 72:866–73. [PubMed: 2211774]
28. Paschalis EP, Verdelis K, Doty SB, Boskey AL, Mendelsohn R, Yamauchi M. Spectroscopic characterization of collagen cross-links in bone. J Bone Miner Res. 2001; 16:1821–8. [PubMed: 11585346]
29. Gourion-Arsiquaud S, Faibish D, Myers E, et al. Use of FTIR spectroscopic imaging to identify parameters associated with fragility fracture. J Bone Miner Res. 2009; 24:1565–71. [PubMed: 19419303]
30. Dehring KA, Crane NJ, Smukler AR, McHugh JB, Roessler BJ, Morris MD. Identifying chemical changes in subchondral bone taken from murine knee joints using Raman spectroscopy. Appl Spectrosc. 2006; 60:1134–41. [PubMed: 17059665]
31. Turunen MJ, Saarakkala S, Rieppo L, Helminen HJ, Jurvelin JS, Isaksson H. Comparison between infrared and Raman spectroscopic analysis of maturing rabbit cortical bone. Appl Spectrosc. 2011; 65:595–603. [PubMed: 21639980]
32. Camacho NP, West P, Torzilli PA, Mendelsohn R. FTIR microscopic imaging of collagen and proteoglycan in bovine cartilage. Biopolymers. 2001; 62:1–8. [PubMed: 11135186]
33. vid-Vaudey E, Burghardt A, Keshari K, Brouchet A, Ries M, Majumdar S. Fourier transform infrared imaging of focal lesions in human osteoarthritic cartilage. Eur Cell Mater. 2005; 10:51–60. [PubMed: 16307426]
34. Xia Y, Ramakrishnan N, Bidthanapally A. The depth-dependent anisotropy of articular cartilage by Fourier-transform infrared imaging (FTIRI). Osteoarthritis Cartilage. 2007; 15:780–8. [PubMed: 17317225]
35. Ramakrishnan N, Xia Y, Bidthanapally A. Fourier-transform infrared anisotropy in cross and parallel sections of tendon and articular cartilage. J Orthop Surg Res. 2008; 3:48. [PubMed: 18837979]
36. Kobrina Y, Rieppo L, Saarakkala S, Jurvelin JS, Isaksson H. Clustering of infrared spectra reveals histological zones in intact articular cartilage. Osteoarthritis Cartilage. 2012; 20:460–48. [PubMed: 22333731]
37. Bonifacio A, Beleites C, Vittur F, et al. Chemical imaging of articular cartilage sections with Raman mapping, employing uni- and multivariate methods for data analysis. Analyst. 2010; 135:3193–204. [PubMed: 20967391]

Author Manuscript Author Manuscript Author Manuscript Author Manuscript

38. Lim NS, Hamed Z, Yeow CH, Chan C, Huang Z. Early detection of biomolecular changes in disrupted porcine cartilage using polarized Raman spectroscopy. J Biomed Opt. 2011; 16:017003. [PubMed: 21280924]
39. Hanifi A, Richardson JB, Kuiper JH, Roberts S, Pleshko N. Clinical outcome of autologous chondrocyte implantation is correlated with infrared spectroscopic imaging-derived parameters. Osteoarthritis Cartilage. 2012; 20:988–6. [PubMed: 22659601]
40. Spalazzi JP, Boskey AL, Camacho NP, Lu HH. Characterization of matrix and mineral content at the neonatal bovine anterior cruciate ligament-to-bone insertion site. PLoS One. 2013; 8(9):e74349. [PubMed: 24019964]
41. Wopenka B, Kent A, Pasteris JD, Yoon Y, Thomopoulos S. The tendon-to-bone transition of the rotator cuff: a preliminary Raman spectroscopic study documenting the gradual mineralization across the insertion in rat tissue samples. Appl Spectrosc. 2008; 62:1285–94. [PubMed: 19094386]
42. Schwartz AG, Pasteris JD, Genin GM, Daulton TL, Thomopoulos S. Mineral distributions at the developing tendon enthesis. PLoS One. 2012; 7:e48630. [PubMed: 23152788]
43. Kim M, Bi X, Horton WE, Spencer RG, Camacho NP. Fourier transform infrared imaging spectroscopic analysis of tissue engineered cartilage: histologic and biochemical correlations. J Biomed Opt. 2005; 10:031105. [PubMed: 16229630]
44. Bi X, Yang X, Bostrom MP, Camacho NP. Fourier transform infrared imaging spectroscopy investigations in the pathogenesis and repair of cartilage. Biochim Biophys Acta. 2006; 1758:934–41. [PubMed: 16815242]
45. Bi X, Li G, Doty SB, Camacho NP. A novel method for determination of collagen orientation in cartilage by Fourier transform infrared imaging spectroscopy (FT-IRIS). Osteoarthritis Cartilage. 2005; 13:1050–8. [PubMed: 16154778]
46. Klein TJ, Chaudhry M, Bae WC, Sah RL. Depth-dependent biomechanical and biochemical properties of fetal, newborn, and tissue-engineered articular cartilage. J Biomech. 2007; 40:182–90. [PubMed: 16387310]
47. Hauselmann HJ, Fernandes RJ, Mok SS, et al. Phenotypic stability of bovine articular chondrocytes after long-term culture in alginate beads. J Cell Sci. 1994; 107(Pt 1):17–27. [PubMed: 8175906]
48. Schinagl RM, Gurskis D, Chen AC, Sah RL. Depth-dependent confined compression modulus of full-thickness bovine articular cartilage. J Orthop Res. 1997; 15:499–506. [PubMed: 9379258]
49. Masuda K, Sah RL, Hejna MJ, Thonar EJ. A novel two-step method for the formation of tissue-engineered cartilage by mature bovine chondrocytes: the alginate-recovered-chondrocyte (ARC) method. J Orthop Res. 2003; 21:139–48. [PubMed: 12507591]
50. Wang CC, Chahine NO, Hung CT, Ateshian GA. Optical determination of anisotropic material properties of bovine articular cartilage in compression. J Biomech. 2003; 36:339–53. [PubMed: 12594982]
51. Wang IE, Mitroo S, Chen FH, Lu HH, Doty SB. Age-dependent changes in matrix composition and organization at the ligament-to-bone insertion. J Orthop Res. 2006; 24:1745–55. [PubMed: 16779829]
52. Hunziker EB, Ludi A, Herrmann W. Preservation of cartilage matrix proteoglycans using cationic dyes chemically related to ruthenium hexaammine trichloride. J Histochem Cytochem. 1992; 40:909–17. [PubMed: 1376743]
53. Erben RG. Embedding of bone samples in methylmethacrylate: an improved method suitable for bone histomorphometry, histochemistry, and immunohistochemistry. J Histochem Cytochem. 1997; 45:307–13. [PubMed: 9016319]
54. Aparicio S, Doty SB, Camacho NP, et al. Optimal methods for processing mineralized tissues for Fourier transform infrared microspectroscopy. Calcif Tissue Int. 2002; 70:422–9. [PubMed: 12055658]
55. Rieppo L, Rieppo J, Jurvelin JS, Saarakkala S. Fourier transform infrared spectroscopic imaging and multivariate regression for prediction of proteoglycan content of articular cartilage. PLoS One. 2012; 7:e32344. [PubMed: 22359683]

Author Manuscript Author Manuscript Author Manuscript Author Manuscript

56. Kim M, Foo LF, Uggen C, et al. Evaluation of early osteochondral defect repair in a rabbit model utilizing Fourier transform-infrared imaging spectroscopy, magnetic resonance imaging, and quantitative T2 mapping. Tissue Eng Part C Methods. 2010; 16:355–64. [PubMed: 19586313]
57. Boskey AL, Posner AS. Bone structure, composition, and mineralization. Orthop Clin North Am. 1984; 15:597–612. [PubMed: 6387574]
58. Mbuyi-Muamba JM, Dequeker J. Biochemical anatomy of human bone: comparative study of compact and spongy bone in femur, rib and iliac crest. Acta Anat (Basel). 1987; 128:184–7. [PubMed: 3107332]
59. Julkunen P, Harjula T, Iivarinen J, et al. Biomechanical, biochemical and structural correlations in immature and mature rabbit articular cartilage. Osteoarthritis Cartilage. 2009; 17:1628–38. [PubMed: 19615962]
60. Clark JM, Norman A, Notzli H. Postnatal development of the collagen matrix in rabbit tibial plateau articular cartilage. J Anat. 1997; 191(Pt 2):215–21. [PubMed: 9306198]
61. Wilson W, Driessen NJ, van Donkelaar CC, Ito K. Prediction of collagen orientation in articular cartilage by a collagen remodeling algorithm. Osteoarthritis Cartilage. 2006; 14:1196–202. [PubMed: 16797194]
62. Gupta HS, Schratter S, Tesch W, et al. Two different correlations between nanoindentation modulus and mineral content in the bone-cartilage interface. J Struct Biol. 2005; 149:138–48. [PubMed: 15681230]
63. Williamson AK, Chen AC, Masuda K, Thonar EJ, Sah RL. Tensile mechanical properties of bovine articular cartilage: variations with growth and relationships to collagen network components. J Orthop Res. 2003; 21:872–80. [PubMed: 12919876]
64. Zhu W, Mow VC, Koob TJ, Eyre DR. Viscoelastic shear properties of articular cartilage and the effects of glycosidase treatments. J Orthop Res. 1993; 11:771–81. [PubMed: 8283321]
65. Ferguson VL, Bushby AJ, Boyde A. Nanomechanical properties and mineral concentration in articular calcified cartilage and subchondral bone. J Anat. 2003; 203:191–202. [PubMed: 12924819]
66. Khanarian NT, Jiang J, Wan LQ, Mow VC, Lu HH. A hydrogel-mineral composite scaffold for osteochondral interface tissue engineering. Tissue Eng Part A. 2012; 18:533–45. [PubMed: 21919797]
67. Khanarian NT, Haney NM, Burga RA, Lu HH. A functional agarose-hydroxyapatite scaffold for osteochondral interface regeneration. Biomaterials. 2012; 33:5247–58. [PubMed: 22531222]

Author Manuscript Author Manuscript Author Manuscript Author Manuscript

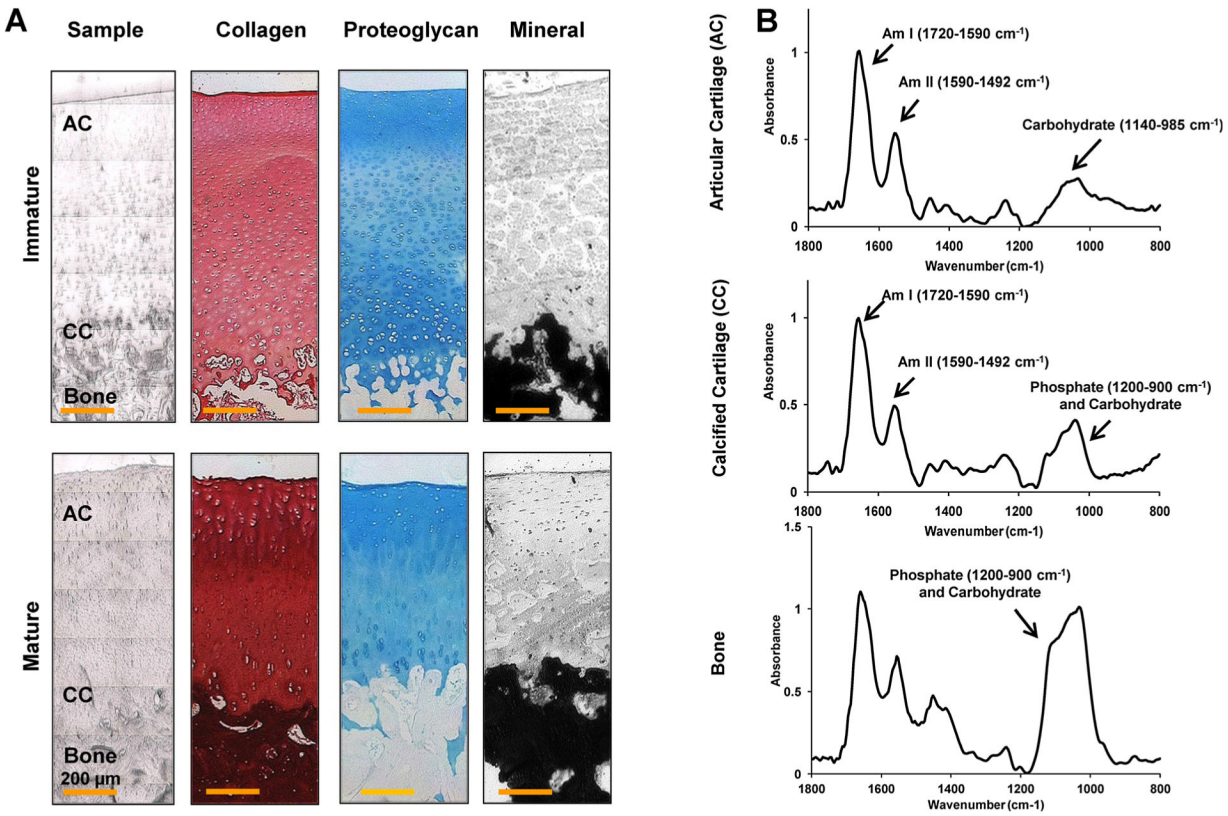

Fig. 1.

Cartilage-to-bone junction. Immature and mature osteochondral samples exhibit region-dependent changes in (*A*) matrix distribution ($n = 3$, picrosirius red for collagen, alcian blue for proteoglycan, von Kossa for mineral, 5×, scale bar = 200μm). (*B*) Characteristic IR spectrum for each tissue region (articular cartilage [AC], calcified cartilage [CC], bone) in immature samples. Note Amide I and II (Am I andAmII) peaks are indicative for collagen, the carbohydrate peak for proteoglycan, and phosphate peak for mineral.

Author Manuscript Author Manuscript Author Manuscript Author Manuscript

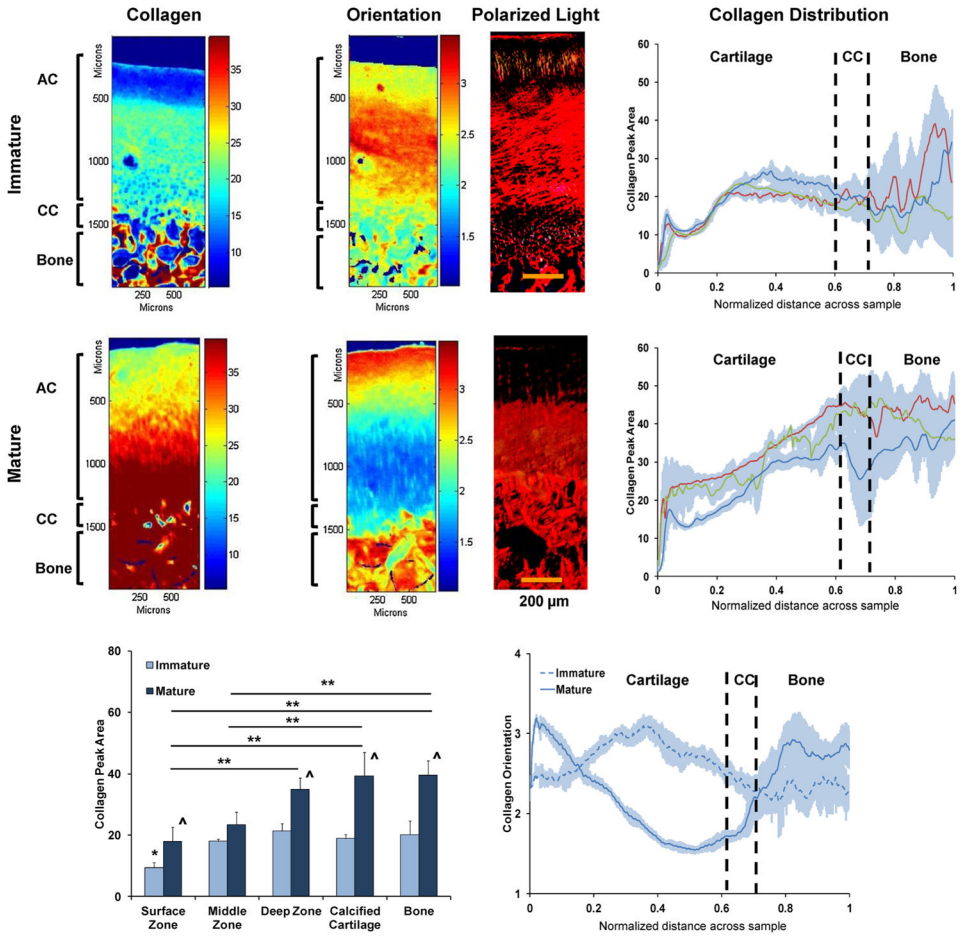

Fig. 2.

Collagen content, distribution, and organization. Peak integration maps ($n = 3$) of amide I show relative collagen content and distribution. Line scans across the cartilage-to-bone junction reveal a stepwise increase in collagen content for immature specimens and a gradual increase for mature specimens (articular cartilage [AC], calcified cartilage [CC]). Peak integration maps ($n = 3$) of the amide I, normalized by amide II, show collagen orientation (blue = perpendicular to polarizer, yellow = mixed orientation, red = parallel to polarizer). Corresponding line scans of collagen orientation show an increase in alignment in the surface zone and deep zone of mature cartilage compared with immature cartilage. Comparison of immature and mature collagen content ($n = 3$, $^{*}p < 0.05$, differences between zones/regions for immature samples; $^{**}p < 0.05$, differences between zones/regions for mature samples; $\wedge p < 0.05$, differences between corresponding immature and mature zones/regions).

Author Manuscript
Author Manuscript
Author Manuscript
Author Manuscript

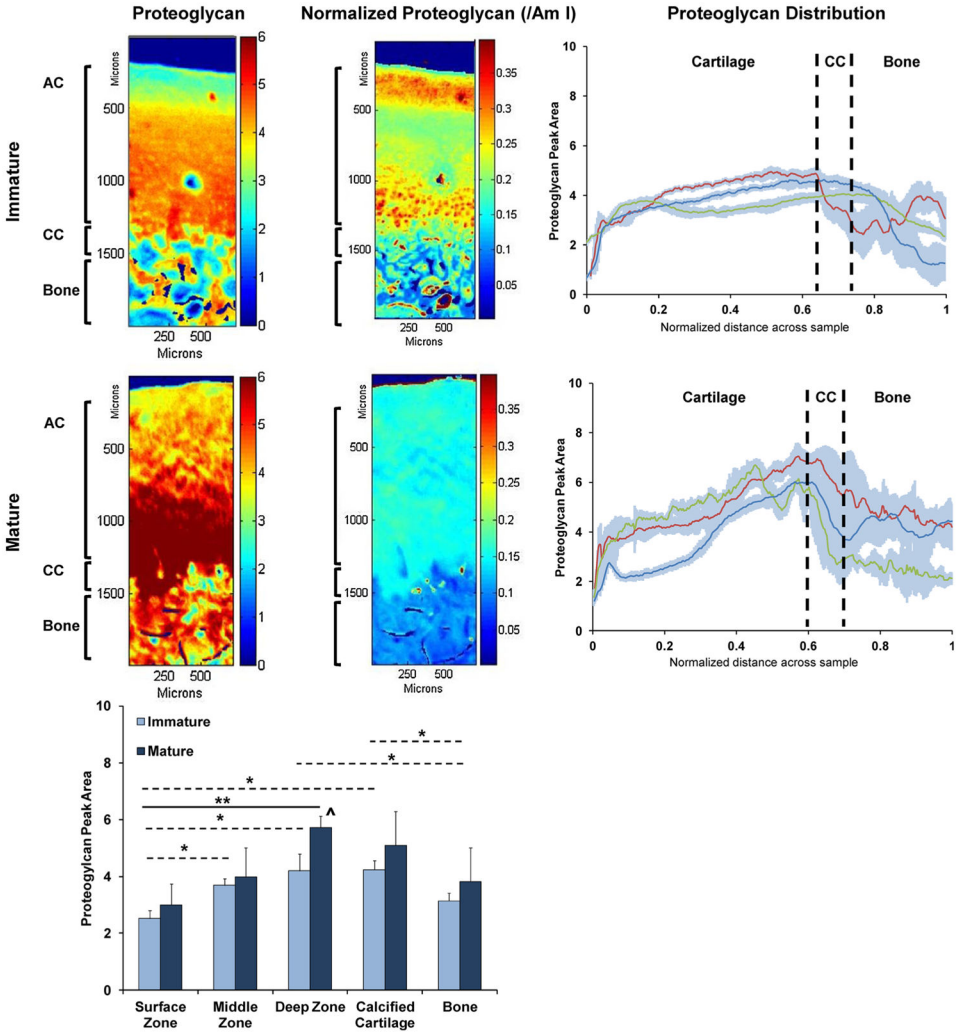

Fig. 3.

Proteoglycan content and distribution. Peak integration maps ($n = 3$) of the carbohydrate band and normalized carbohydrate band show relative proteoglycan distribution. Line scans across the cartilage-to-bone junction reveal a peak in non-normalized proteoglycan content in deep zone cartilage for both immature and mature specimens (articular cartilage [AC], calcified cartilage [CC]). Comparison of immature and mature proteoglycan content ($n = 3$, $^{*}p < 0.05$, differences between zones/regions for immature samples; $^{**}p < 0.05$, differences between zones/regions for mature samples; $\wedge p < 0.05$, differences between corresponding immature and mature zones/regions).

Author Manuscript Author Manuscript Author Manuscript Author Manuscript

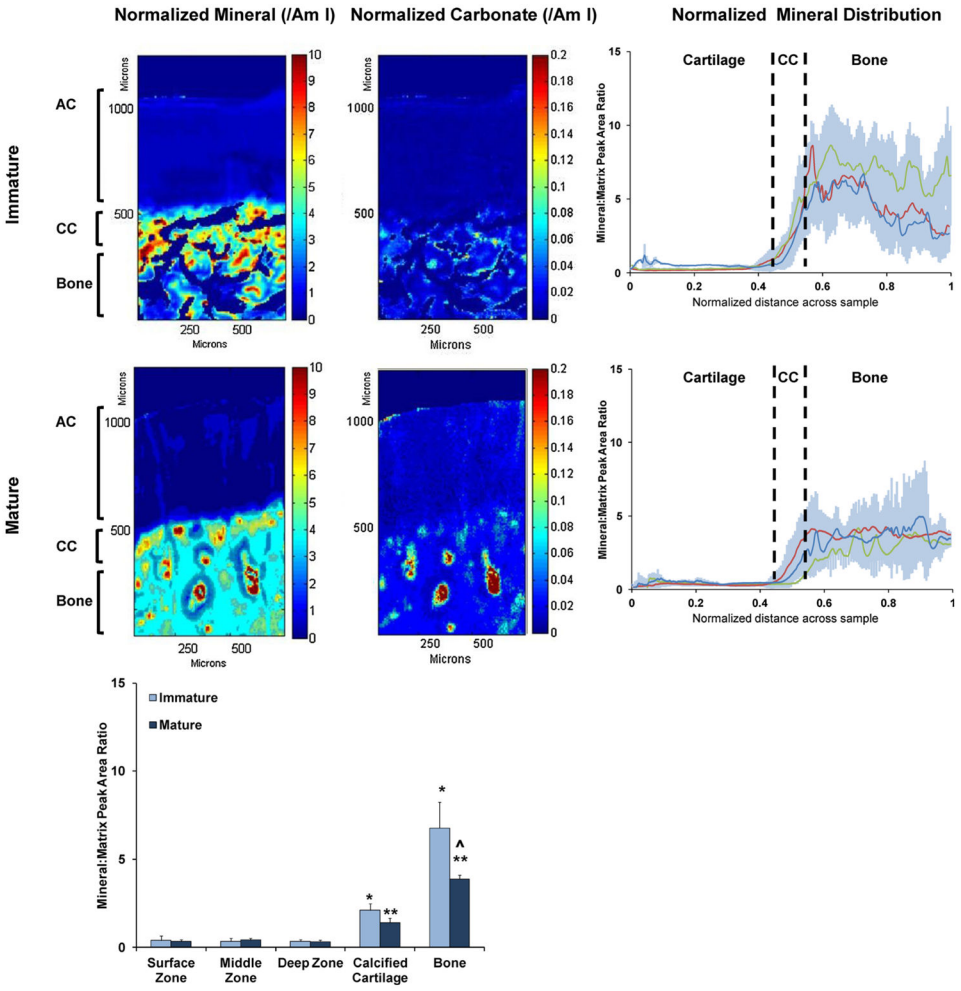

Fig. 4.

Mineral content and distribution. Peak integration maps ($n = 3$) of the phosphate band, normalized by amide I, show relative mineral distribution. Peak integration maps ($n = 3$) of the carbonate band, normalized by amide I, show carbonate distribution. Line scans across the cartilage-to-bone junction reveal a distinct transition from mineral-free to mineral-rich tissue regions for both immature and mature specimens (articular cartilage [AC], calcified cartilage [CC], Am I-Amide I). Comparison of immature and mature mineral content ($^{*}p < 0.05$, differences between zones/regions for immature samples; $^{**}p < 0.05$, differences between zones/regions for mature samples; $\wedge p < 0.05$, differences between corresponding immature and mature zones/regions).

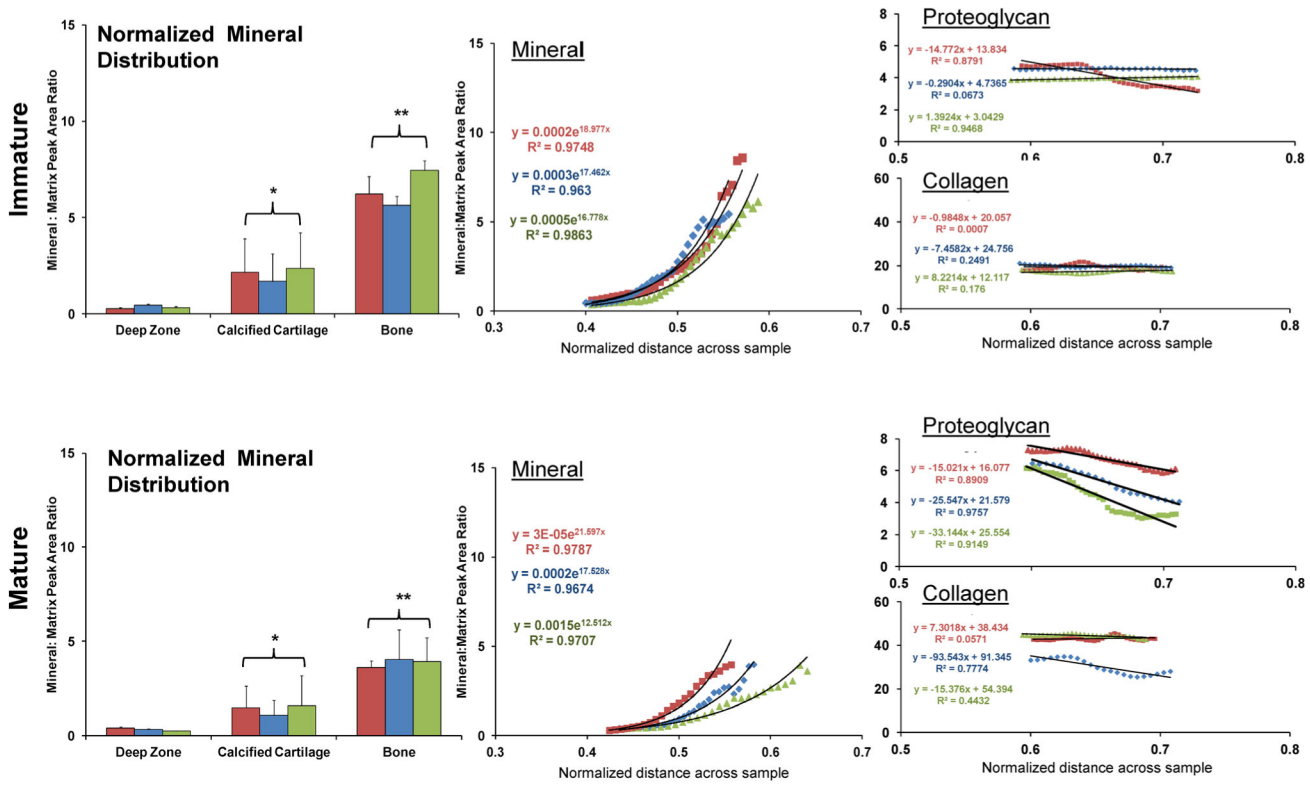

Fig. 5.

Matrix distribution across interface. Results from three different joints (red, blue, and green) are compared for each age group. The normalized phosphate content of the transition region is intermediate between deep zone uncalcified cartilage and bone ($^{*}p < 0.05$, difference with uncalcified cartilage; $^{**}p < 0.05$, difference with both uncalcified cartilage and calcified cartilage). Linear regression analyses of region-dependent distribution of matrix components reveal relatively linear fits for collagen and proteoglycan regardless of age, whereas an exponential mineral gradient was observed in immature and mature samples.

Author Manuscript Author Manuscript Author Manuscript Author Manuscript